International Journal of Rock Mechanics & Mining Sciences 79 (2015) 193–204

Contents lists available at ScienceDirect

International Journal of Rock Mechanics & Mining Sciences

journal homepage: www.elsevier.com/locate/ijrmms

Improved analytical solutions for the response of underground excavations in rock masses satisfying the generalized Hoek–Brown failure criterion

Fabrice Rojat [a,*], Vincent Labiouse [b], Philippe Mestat [c]

[a] Centre d'Études et d'Expertise sur les Risques, l'Environnement, la Mobilité et l'Aménagement, Bron, France
[b] École Polytechnique Fédérale de Lausanne-Laboratoire de Mécanique des Roches, Lausanne, Switzerland
[c] Institut Français des Sciences et Technologies des Transports, Paris, France

ARTICLE INFO

Article history:
Received 28 February 2014
Received in revised form
17 July 2015
Accepted 8 August 2015

Keywords:
Tunnel
Generalized Hoek–Brown criterion
Convergence
Analytical solutions
Normalized criterion
Edge effects

ABSTRACT

Analytical solutions for tunnel design are widely used in practical engineering, as they allow a quick analysis of design issues such as estimation of support requirement. In recent years, several papers analyzing the behavior of rock masses that obey the conventional or generalized Hoek–Brown criterion have been published. This article presents a complementary analysis that includes a new normalization of the generalized Hoek–Brown failure criterion, complete solutions for associated and non-associated flow rules, with some new closed-form solutions in the latter case, and in-depth considerations regarding intermediate stresses and edge effects. The results obtained show full agreement with existing solutions in the literature, when possible, and with numerical finite element models in cases that had not been treated previously.

1. Introduction

Major civil engineering projects such as tunnels at depth pose significant challenges to soil and rock mechanics engineers alike. During the design stage, these types of projects require systematic treatment by engineers, who, among others, have to develop a geotechnical model of the site, optimize the design, and assess the uncertainties and risks in the short- and long-term life of the project[1]. To do this, the geotechnical engineer seeks to identify the physical properties that significantly influence the mechanical behavior of the rock mass, based on site surveys, core analyses, and laboratory tests on rock samples. Then, the engineer relies on both empirical and theoretical approaches to include all of this technical data into a calculation process for design. The ultimate goal is to determine a safe and financially acceptable solution that is compatible with all the constraints applicable to the project. In the end, the construction phase provides an insight into the real behavior of the ground and may allow the geotechnical engineer to identify defects in the model, adjust the design, and gain experience.

The case of tunnels fits this description well since, when they are not self-stable, underground works are characterized by a significant interaction between the stabilizing structures and the surrounding geological material. Consequently, the relevance of the geotechnical model depends strongly on its ability to take into account two major uncertainties: variability in material properties and representativeness of calculation processes. In this context, simplified design methods such as convergence-confinement are worth using, as they allow a quick and reasonable assessment of tunnel support and may be used for sensitivity studies. As such, they can be part of improvements in tunnel design, as they facilitate exploration of the possible range of stability conditions around the excavation.

Many authors have proposed analytical or semi-analytical solutions for establishing the ground characteristic curves that describe the behavior of a rock mass affected by tunnel excavation. Most often, these solutions rely on hypotheses that allow an axisymetric approach (circular tunnel at great depth in an isotropic and homogeneous material, with an isotropic initial stress field and conditions for plane strain), and tunnel excavation is modeled by decreasing a fictitious internal pressure applied to tunnel periphery. These solutions may consider various material models (linear or non-linear elasticity, failure criteria, etc.). For instance, more than 30 years ago, Brown et al.[2] could already refer to 22 significant contributions on this subject made since Fenner's early

* Correspondence to: Centre d'Études et d'Expertise sur les Risques, l'Environnement, la Mobilité et l'Aménagement Laboratoire de Lyon, 25 Avenue François Mitterrand, 69674 Bron, France.
E-mail address: fabrice.rojat@cerema.fr (F. Rojat).

http://dx.doi.org/10.1016/j.ijrmms.2015.08.002
1365-1609/

work[3]. In recent years, significant work has been undertaken to obtain more ready-to-use mathematical formulations for ground characteristic curves, including the well-known generalized Hoek–Brown failure criterion. These developments are of particular interest because the Hoek–Brown criterion may be used in a wide range of situations for underground works, including fractured hard rocks but also materials such as hard soils – soft rocks (see Refs. 4 and 5 for instance).

Generally speaking, the plastic formulations used in these theoretical developments can be divided into those for which stress–strain relationships are based on the incremental or flow theory of plasticity (IS, for "incremental strain") and those based on the deformation or total strain theory of plasticity (TS, for "total strain"). The IS formulations relate stress to plastic strain increments and therefore involve 'time variables' (through kinematic parameters) in addition to usual space variables. As a result, the IS formulation requires solving partial differential equations or alternatively, in problems such as the one to be solved in this article, transformation of these partial differential equations into total differential equations that can be solved in closed-form. In contrast, the TS formulations relate stresses to total plastic strains and do not involve a 'time variable': as a result, for problems involving one space variable only, as in the case of the problem addressed in this paper, they require solving total differential equations only (from a mathematical point of view, the TS formulation is usually significantly simpler than the IS formulation). Although both types of formulations yield the same results in simple problems involving mononotic progression of loading/unloading, as in the case of the problem addressed in this work, the IS formulation is supposed to be more rigorous and more general than the TS formulation because it can be applied to solve plastic problems which do not necessarily involve mononotic progression of loading/unloading. Moreover, a TS formulation may be difficult to express in the case of non-linear flow rules (such as associated Hoek–Brown).

Subsequent to the first analysis from Brown et al.[2], in which several simplifications were considered (no elastic strain within the plastic radius for instance), three important results can be cited. First, Carranza-Torres et al.[6] and Carranza-Torres[7] described a full and rigorous solution with both original and generalized Hoek–Brown criteria, with associated or non-associated flow rules, and perfectly plastic or brittle-plastic behaviors. They used the IS formulation for plasticity, but obtained total differential equations with ingenious variable changes. Shortly thereafter, Sharan[8–10] proposed an alternative solving process with a TS formulation, limited to the case of a Mohr–Coulomb flow rule, and yielding comparable results. Finally, Serrano et al.[11] described an additional solving method using a general expression of the failure criterion (written in terms of Lambe variables) and of a non-associated flow rule (including a stress-dependant dilatancy). They used TS plasticity, and their results matched well with the aforementioned works in the case of a Hoek–Brown failure envelope.

However, despite the reliability of this scientific work, the authors noted that improvements could still be suggested for ground characteristics curves in a rock mass obeying the generalized Hoek–Brown criterion. In particular, a new normalization of the criterion leading to simplified equations is presented in the next sections. Moreover, the problem of edge effects on the failure surface is fully addressed, allowing one to evaluate its influence on the description of rock mass behavior. A new closed-form solution is also presented in the case of an associated flow rule, using IS plasticity and variable changes.

2. Description of the problem and governing equations

The calculation process described below relies mainly on the approach proposed in Refs. 6 and 7, with several improvements as mentioned in the previous section. The hypotheses are as follows.

2.1. Problem description in the context of the convergence-confinement method

The convergence-confinement method (also called the method of characteristic curves) is aimed at describing as precisely as possible the principle of interaction between a rock mass and a tunnel support. It allows for taking into account the "work" of the rock mass, during the design process, since this work contributes to the stability of the excavation. The description of ground behavior is based on a direct integration of mechanical equations, thus requiring some simplifying hypotheses.

First, the problem has to be studied in an axisymetric configuration, which implies several assumptions. The rock mass must be considered as homogeneous and isotropic, with isotropic initial stress conditions. The excavation must be circular and at great depth (at least 10 times the tunnel radius), so as to be able to disregard the influence of gravitational and side effects. Moreover, the tunnel has to be long enough to assume a plane strain state (i.e. $\varepsilon_x=0$, with x being oriented towards the longitudinal axis of the tunnel). Using these hypotheses, the principle of the convergence-confinement method can be summarized according to the diagram shown in Fig. 1.

During the excavation process, convergence begins ahead of the tunnel face (see Ref. 13 or 14, for example) and maximum displacement is not obtained immediately after the excavation phase. This variation of convergence with advance is usually referred to as the longitudinal displacement profile LDP. For a non-supported tunnel, the convergence-confinement method represents the effect of the advancing tunnel face via a fictitious internal pressure σ_i applied to the tunnel walls which decreases progressively from the initial stress in situ σ_0 to zero when the plane strain state is obtained. The ground reaction curve (or convergence curve) GRC, which can be calculated using closed-form

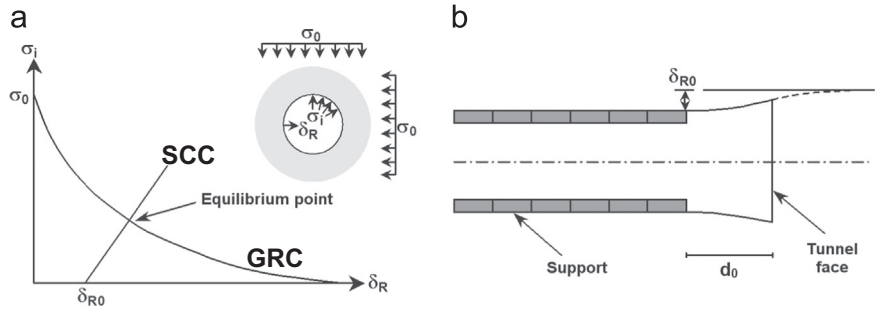

Fig. 1. Schematic representation of the basis of the convergence-confinement method (after Ref. 12): (a) shows how the equilibrium point is obtained; while (b) represents the convergence process due to tunnel face advance and the definition of parameters d_0 and d_{R0}.

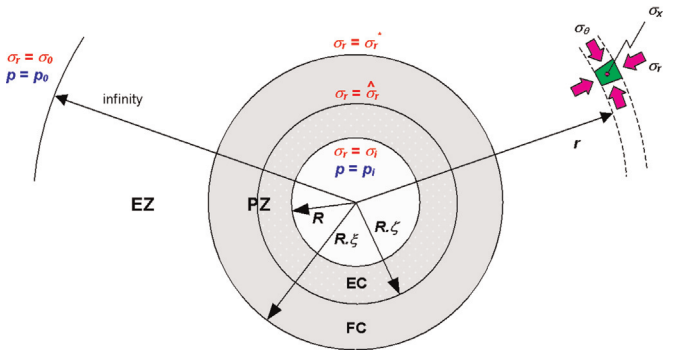

Fig. 2. Configuration studied in this paper for the calculation of ground characteristic curves (EZ=Elastic Zone, PZ=Plastic Zone, EC=Criterion Edge, FC=Criterion Face).

solutions for simple models of ground behavior, represents the rock mass response to this unloading process. When a support is installed, its response to wall displacements is represented by a support characteristic curve (or confinement curve) SCC that intersects the GRC at the theoretical final equilibrium point. The origin of the support characteristic curve is the initial displacement at tunnel wall δ_{R0}, which depends in particular on the distance to tunnel face d_0.

This paper deals solely with calculating the ground reaction curve GRC in the case of a Hoek–Brown failure criterion. For the calculation of the support characteristic curve SCC and the longitudinal displacement profile LDP, readers are referred to Refs. 15–18 in particular. Interesting complementary approaches, for other material models, can be found also in Refs. 19–21.

According to the convergence-confinement method theory, analysis of the stress and strain conditions around the tunnel can be approached via a system of cylindrical coordinates, as gradients may only appear in the radial direction. The general configuration studied here is summarized in Fig. 2.

Indices r, θ and x are for radial, tangential and longitudinal directions, respectively. The normal stresses acting on an infinitesimal element at a distance r from the tunnel center are called σ_r, σ_θ, and σ_x. The strains in the same directions are ε_r, ε_θ, and ε_x. Stresses and strains are positive in compression, and the radial displacement, u, is positive towards the tunnel center.

From the initial condition of isotropic stress σ_0, the decreasing internal pressure σ_i at the tunnel walls induces a stress field where the major principal stress σ_1 is σ_θ (tangential), the intermediate principal stress σ_2 is σ_x (longitudinal), and the minor principal stress σ_3 is σ_r (radial).

The reduction of σ_i causes the stress deviator to increase near the tunnel walls, which may lead to ground plastification. The plastic zone is cylindrical (symmetry condition) and is limited by a plastic radius $R\xi$, corresponding to a radial stress σ_r^*. Within the plastic zone, edge effects may appear, delineated by a radius $R\zeta$ and a radial stress $\hat{\sigma}_r$ (see Section 2.5). When stress conditions remain in the field of elasticity for the rock mass, $R\xi$ is equal to R, i.e. $\xi=1$, and naturally $\zeta=1$ also.

Due to symmetry of the problem, the equations described in the next sections are expressed using a cylindrical reference system. For the sake of simplicity, normalized expressions of the governing equations are used, as already done in Refs. 6 and 7, with the variations discussed below.

2.2. A new normalized expression of the failure criterion

Analytical solutions with the generalized Hoek–Brown failure criterion usually result in complex mathematical formulations that may be difficult to handle or may cause errors in the solving process. In order to facilitate the representation of the criterion in the Mohr plane, Londe[22] noted that its original expression could be transformed into

$$S_1 = S_3 + (S_3)^{\frac{1}{2}} \text{ with: } \quad S_j = \frac{\sigma_j}{m\,\sigma_{ci}} + \frac{s}{m^2} \quad (j \in \{1, 3\}) \tag{1}$$

where σ_j are the major and minor principal stresses, m and s are the Hoek–Brown parameters, and S_j are the normalized major and minor principal stresses ($j \in \{1, 3\}$).

Carranza-Torres[7] extended this proposition to include the generalized form of the criterion (with exponent α instead of ½) and obtained an expression with two apparent parameters:

$$S_1 = S_3 + \mu_{HB} \cdot S_3^{\alpha} \tag{2}$$

In fact, this expression can be improved by eliminating the μ_{HB} variable. In this paper, the major and minor principal stresses are normalized with the new normalization equation below ($0.5 < \alpha < 1$):

$$S_j = \frac{\sigma_j}{m^{\frac{\alpha}{1-\alpha}}\sigma_{ci}} + \frac{s}{m^{\frac{1}{1-\alpha}}} \tag{3}$$

As a consequence, the generalized failure criterion

$$\sigma_1 = \sigma_3 + \sigma_{ci}\left(m\,\frac{\sigma_3}{\sigma_{ci}} + s\right)^{\alpha} \tag{4}$$

takes the simplified normalized form

$$S_1 = S_3 + (S_3)^{\alpha} \tag{5}$$

These formulae allow handling the failure criterion with only one apparent parameter α. With the axisymetric geometry studied in this paper (see Section 2.1), the criterion finally takes the form

$$S_\theta = S_r + (S_r)^{\alpha} \tag{6}$$

This normalization process can be used to simplify all equations governing the mechanical problem, in particular plasticity equations (flow rule, consistency equation) and behavior equations (equilibrium equation, Hooke's law, strain–displacement relationships).

2.3. Normalized plasticity equations

With regard to the plastic flow rule and consistency equations, the usual form of the theory of incremental plasticity is used in this paper. The domain of reversible behavior is considered to be limited by a failure envelope $\mathcal{F}$ that is dependent on the stress tensor $\underline{\sigma}$. During the elastic phase $\mathcal{F}(\underline{\sigma}) < 0$; and plasticity appears when $\mathcal{F}(\underline{\sigma}) = 0$. For instance, given the assumptions of Section 2.1, the Hoek–Brown failure envelope can be defined as

$$\mathcal{F}(\underline{\sigma}) = \sigma_\theta - \sigma_r - \sigma_{ci}\left(m\frac{\sigma_r}{\sigma_{ci}} + s\right)^{\alpha} \tag{7}$$

or in normalized form as

$$F = S_\theta - S_r - (S_r)^{\alpha} \tag{8}$$

In the case of perfect plasticity, as considered in this paper, the failure envelope is not modified by the stress increments and the stress tensor remains on the failure surface. This behavior is expressed by the consistency equation

$$\dot{\mathcal{F}}(\underline{\sigma}, \dot{\underline{\sigma}}) = \frac{\partial \mathcal{F}}{\partial \underline{\sigma}} : \dot{\underline{\sigma}} = 0 \tag{9}$$

where "•" is an operator indicating the derivative with respect to a kinematic parameter (or 'time variable') that characterizes the infinitesimal evolution of the system.

As the parameters σ_{ci}, s, m, and α of the failure criterion do not depend on the kinematic parameter, it can be stated that

$$\dot{\sigma}_r = \dot{S}_r \cdot \sigma_{ci} \cdot m^{\alpha/(1-\alpha)} \tag{10}$$

which easily demonstrates that the consistency equation can be rewritten with normalized stresses as

$$\frac{\partial F}{\partial S_r}\dot{S}_r + \frac{\partial F}{\partial S_\theta}\dot{S}_\theta = 0 \tag{11}$$

Moreover, when plasticity appears, inelastic strains begin to accumulate and the strain tensor is usually broken down into two parts

$$\underline{\underline{\varepsilon}} = \underline{\underline{\varepsilon}}^{el} + \underline{\underline{\varepsilon}}^{P} \tag{12}$$

with ε^{el} the elastic strain tensor that obeys Hooke's law (see below), and ε^{P} the plastic strain tensor. The plastic flow rule allows defining the plastic strain rate as a function of a plastic potential $\mathcal{G}$

$$\underline{\underline{\dot{\varepsilon}}}^{P} = \dot{\chi}\frac{\partial \mathcal{G}}{\partial \underline{\underline{\sigma}}} \tag{13}$$

with $\dot{\chi}$ a plastic multiplier. The flow rule is called "associated" when $\mathcal{G} = \mathcal{F}$.

In this paper, two plastic flow rules are considered (expressed in normalized stresses). In the associated case, a Hoek–Brown potential is used:

$$G^{P}_{HB} = F = S_\theta - S_r - (S_r)^{\alpha} \tag{14}$$

In the non-associated case, a Mohr–Coulomb potential is taken into account, with a dilatancy ψ :

$$G^{P}_{MC} = S_\theta - K_\psi S_r \tag{15}$$

where $K_\psi = \frac{1+\sin(\psi)}{1-\sin(\psi)}$.

It can be easily shown in this case that the plastic flow rule (13) is equivalent to the normalized expression

$$\underline{\underline{\dot{\varepsilon}}}^{P} = \dot{\chi}\frac{\partial G^{P}}{\partial \underline{\underline{\sigma}}} \tag{16}$$

where G^P can be defined by Eq. (14) or (15). With the geometry described in Section 2.1, this relationship may be written in cylindrical coordinates as

$$\dot{\varepsilon}^{P}_\theta = \dot{\chi}\frac{\partial G^{P}}{\partial S_\theta}, \quad \dot{\varepsilon}^{P}_x = \dot{\chi}\frac{\partial G^{P}}{\partial S_x} = 0, \quad \dot{\varepsilon}^{P}_r = \dot{\chi}\frac{\partial G}{\partial S_r} \tag{17}$$

With the set of relationships presented in this section, plasticity can be fully described in terms of normalized stresses. In addition, normalized equations concerning equilibrium state and stress–strain–displacement behavior are required to solve the mechanical problem.

2.4. Normalized behavior relationships

If no body forces are considered, which is the case with the assumptions in Section 2.1, the radial and tangential stresses obey the equilibrium equation below

$$\frac{\partial \sigma_r}{\partial r} + \frac{\sigma_r - \sigma_\theta}{r} = 0 \tag{18}$$

This equation can be normalized as follows (after expression (3)) in the axisymetric case of Section 2.1:

$$\frac{\partial S_r}{\partial r} + \frac{S_r - S_\theta}{r} = 0 \tag{19}$$

Likewise, the classical Hooke stress–strain relationships, written in terms of radial and tangential principal stresses, can be transformed into

$$\begin{cases} \varepsilon_r - \varepsilon_r^P = \dfrac{1}{2\Gamma}\left[(1-\nu)(S_r - S_0) - \nu(S_\theta - S_0)\right] \\ \varepsilon_\theta - \varepsilon_\theta^P = \dfrac{1}{2\Gamma}\left[(1-\nu)(S_\theta - S_0) - \nu(S_r - S_0)\right] \\ S_x - S_0 = \nu(S_r - S_0) + \nu(S_\theta - S_0) \end{cases} \tag{20}$$

where ν is the Poisson ratio, Γ is the normalized second Lamé coefficient, $\Gamma = \mu/[\sigma_{ci} m^{\alpha/(1-\alpha)}]$, μ is the second Lamé coefficient, $\mu = E/[2(1+\nu)]$, E is Young's modulus, and $\{S_r, S_\theta, S_x, S_0\}$ are the normalized stresses that replace $\{\sigma_r, \sigma_\theta, \sigma_x, \sigma_0\}$, respectively.

These equations can be completed by the strain–displacement relationships under the assumptions of Section 2.1 (these relationships are not modified by the normalization process)

$$\varepsilon_r = \frac{\partial u}{\partial r} \tag{21}$$

$$\varepsilon_\theta = \frac{u}{r} \tag{22}$$

where u is the radial displacement.

2.5. Additional formulations in the specific case of edge effects

The Hoek–Brown failure criterion or plastic potential exhibit singularities in the σ_1–σ_2–σ_3 stress space, as was shown by Pan et al.[23] in their 3D description of the yield surface. These singularities appear as "edges" when two principal stresses are equal (see Fig. 3). This specific behavior is due to the criterion formulation using only principal stresses σ_1 and σ_3, but not intermediary stress σ_2.

The same statement can be made for the classical Mohr–Coulomb failure criterion or plastic potential. The main problem with edges is that the criterion (or potential) can no longer be derived with respect to stresses, which invalidates some of the equations presented in the previous sections, such as Eq. (16) for instance. The following paragraphs explain how this problem can be handled.

For the configurations studied in this paper, edge effects may only appear in the case of $S_x = S_\theta$. The plastic flow rules can be defined separately on the two adjacent faces of the criterion. On the first face, the plastic potential G_1^P is a function of S_θ and S_r. In this case, the plastic flow rule may be expressed in cylindrical coordinates as

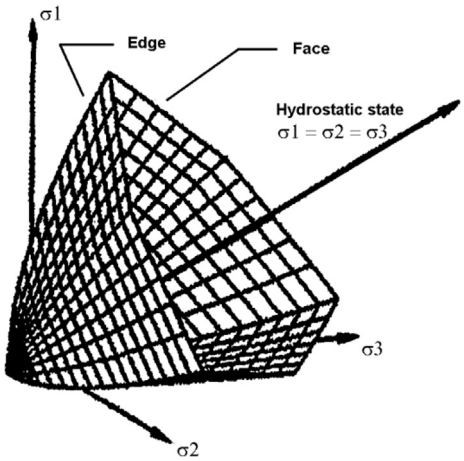

Fig. 3. Hoek–Brown failure criterion in the Haigh–Westergaard stress space, showing the problem of edge effects (modified after Descoeudres[24]).

$$\dot{\varepsilon}_\theta^P = \dot{\chi}_1 \frac{\partial G_1^P}{\partial S_\theta}, \quad \dot{\varepsilon}_x^P = 0, \quad \dot{\varepsilon}_r^P = \dot{\chi}_1 \frac{\partial G_1^P}{\partial S_r} \tag{23}$$

On the second face of the criterion, the plastic potential G_2^P is a function of S_x and S_r. In this case, the plastic flow rule is

$$\dot{\varepsilon}_\theta^P = 0, \quad \dot{\varepsilon}_x^P = \dot{\chi}_2 \frac{\partial G_2^P}{\partial S_x}, \quad \dot{\varepsilon}_r^P = \dot{\chi}_2 \frac{\partial G_2^P}{\partial S_r} \tag{24}$$

On the edge, the convex combination of both plastic rules can be used, yielding the following relationships:

$$\dot{\varepsilon}_\theta^P = \dot{\chi}_1 \frac{\partial G_1^P}{\partial S_\theta}, \quad \dot{\varepsilon}_x^P = \dot{\chi}_2 \frac{\partial G_2^P}{\partial S_x}, \quad \dot{\varepsilon}_r^P = (\dot{\chi}_1 + \dot{\chi}_2)\frac{\partial G^P}{\partial S_r} \tag{25}$$

with $\frac{\partial G^P}{\partial S_r} = \frac{\partial G_1^P}{\partial S_r} = \frac{\partial G_2^P}{\partial S_r}$

Eq. (25) shows that the dual contribution of the two adjacent faces of the plastic potential results in increased plastic deformations when edge effects appear. Another consequence of edge effects is that (for the plastic potentials considered here) $\dot{\varepsilon}_x^P = \dot{\varepsilon}_\theta^P \neq 0$, which means that $\varepsilon_x^P \neq 0$ and $\varepsilon_x^{el} \neq 0$ as the condition of plane strain $\varepsilon_x = 0$ remains valid. Equation set (20), which expresses a form of the generalized Hooke's law for the geometry studied in this paper, can be replaced by

$$\begin{cases} \varepsilon_r - \varepsilon_r^P = \dfrac{1}{H}\left[(S_r - S_0) - 2\nu(S_\theta - S_0)\right] \\ \varepsilon_\theta - \varepsilon_\theta^P = \dfrac{1}{H}\left[(1-\nu)(S_\theta - S_0) - \nu(S_r - S_0)\right] \\ \varepsilon_x - \varepsilon_x^P = \varepsilon_\theta - \varepsilon_\theta^P \end{cases} \tag{26}$$

where H is a the normalized Young modulus, $H = E/[\sigma_{ci} m^{\alpha/(1-\alpha)}]$.

Eqs. (4)–(26) describe a complete mathematical framework, with normalized stresses, for the analysis of tunnel convergence when the generalized Hoek–Brown failure criterion is used. Closed-form solutions can be developed, as presented below.

3. Analytical solutions for ground characteristic curves

The analytical solutions that follow are presented in several steps. First, known solutions for the elastic zone are given (Section 3.1). Next, calculations for the plastic zone without edge effects are explained in two sections: the first section describes stresses in the plastic zone and its extent (Section 3.2), while the second describes the strains and displacements (Section 3.3). Finally, the case of edge effects is analyzed, again in two parts (Sections 3.4 and 3.5).

3.1. Solutions for the elastic zone

The elastic zone is located beyond the plastic radius $R\xi$. In this section, the stress value $\sigma_r(r = R.\ \xi) = \sigma_r^*$ is assumed to be already known. Consequently the boundary conditions for the plastic zone are

$$\text{at } r = R\xi: \quad \sigma_r = \sigma_r^* (\text{or } S_r = S_r^*) \tag{27}$$

$$\text{when } r \to +\infty: \quad \sigma_r = \sigma_0 (\text{or } S_r = S_0) \tag{28}$$

The problem in this case was solved by Lamé[25]. The solution can be obtained by combining Eqs. (19) and (20) with $\varepsilon_r^P = \varepsilon_\theta^P = 0$, (21), (22) and the boundary conditions above, which yields

$$S_r = S_0 - (S_0 - S_r^*)\left(\frac{R\xi}{r}\right)^2 \tag{29}$$

$$S_\theta = S_0 + (S_0 - S_r^*)\left(\frac{R\xi}{r}\right)^2 \tag{30}$$

$$\varepsilon_r = -\frac{1}{2\Gamma}(S_0 - S_r^*)\left(\frac{R\xi}{r}\right)^2 \tag{31}$$

$$\varepsilon_\theta = \frac{1}{2\Gamma}(S_0 - S_r^*)\left(\frac{R\xi}{r}\right)^2 \tag{32}$$

$$u = \frac{1}{2\Gamma}(S_0 - S_r^*)\frac{(R\xi)^2}{r} \tag{33}$$

where S_0 and S_r^* are obtained from σ_0 to σ_r^* after transformation given by Eq. (3).

Since $S_r + S_\theta = 2S_0$ after expressions (29) and (30), the value of the normalized intermediary stress S_x can be easily deduced from Eq. (20):

$$S_x = S_0 \tag{34}$$

If no plastic zone appears around the tunnel, the stress and strain field can be easily inferred by replacing σ_r^* by σ_i in the equations above.

3.2. Plastic zone without edge effects: solutions for stresses and plastic radius

As mentioned before, the elastoplastic case when no edge effects appear was rigorously addressed by Carranza-Torres[7] and Sharan[10]. However, some improvements can be proposed: consequently, the following calculations follow the same path as in Ref. 7, but improve on them by calculating the values of the intermediate principal stress and by offering a new closed-form solution in the case of an associated flow rule. The additional solutions in the case of edge effects are presented in Sections 3.4 and 3.5.

In order to solve the governing equations for the plastic zone, appropriate boundary conditions must be defined. In the configuration studied here (see Section 2.1), they are as follows:

$$\text{at } r = R\xi \quad \sigma_r = \sigma_r^* (\text{or } S_r = S_r^*) \tag{27}$$

$$\text{at } r = R: \quad \sigma_r = \sigma_i \ (\text{or } S_r = S_i) \tag{35}$$

As before, the normalized stress S_r^* at the plastic radius is assumed to be known. Two additional boundary conditions for displacements can be derived from the previous elastic solutions. At $r = R\xi$

$$u = \frac{S_0 - S_r^*}{2\Gamma} R\xi \tag{36}$$

$$\dot{u} = \frac{S_0 - S_r^*}{\Gamma} R \tag{37}$$

With these boundary conditions and the set of governing equations presented in Section 2, the stresses in the plastic zone are calculated first. The equilibrium Eq. (19) and the failure criterion yield for the plastic zone:

$$\frac{\partial S_r}{\partial r} - \frac{S_r^\alpha}{r} = 0 \tag{38}$$

This differential equation can be integrated with the boundary condition (27) to obtain the expression for radial stresses:

$$S_r = \left[(1-\alpha)\ln\left(\frac{r}{R\xi}\right) + S_r^{*1-\alpha}\right]^{\frac{1}{1-\alpha}}, \tag{39}$$

which is similar to the formula obtained in Ref. 7. Next, the tangential stresses can be easily obtained from the failure criterion $S_\theta = S_r + S_r^\alpha$.

The longitudinal stresses will be necessary to identify edge effects in subsequent calculations; these are obtained from Eq. (20):

$$S_x = (1-2\nu)S_0 + \nu\left(2S_r + S_r^\alpha\right) \tag{40}$$

Now that the stress conditions within the plastic zone have been fully described, it is possible to characterize the elastic/plastic limit more precisely by calculating S_r^* and the plastic radius $R\xi$. At any point in the elastic zone the following relationship is verified (from Eqs. (29) and (30)):

$$S_\theta + S_r = 2S_0 \tag{41}$$

This relationship is also valid at the elastic/plastic limit ($r=R\xi$). With the failure criterion $S_\theta = S_r + S_r^\alpha$ it becomes

$$S_r^{*\alpha} + 2S_r^* - 2S_0 = 0 \tag{42}$$

where S_r^* is the normalized radial stress at the elastic/plastic limit. This equation can be solved directly when $\alpha=½$ and yields

$$S^*_{r,\alpha=1/2} = \left[\frac{1-\sqrt{1+16S_0}}{4}\right]^2 \tag{43}$$

When $\alpha\neq½$, there is no exact solution for S_r^*. However, a simple numerical process such as the Newton–Raphson method (usually implemented in commercial spreadsheets) can be used to obtain S_r^*. Sofianos et al.[26] also proposed a good approximation with only one iteration of the Newton–Raphson algorithm, starting from the value obtained when $\alpha=½$:

$$S^*_{r,\alpha\neq1/2} \approx S^*_{r,\alpha=1/2} - \frac{\left(S^*_{r,\alpha=1/2}\right)^\alpha + 2\left(S^*_{r,\alpha=1/2} - S_0\right)}{\alpha\left(S^*_{r,\alpha=1/2}\right)^{\alpha-1} + 2} \tag{44}$$

Once Eq. (42) is solved, the plastic radius can be calculated from expression (39) at $r=R$:

$$S_r = S_i = \left[(1-\alpha)\ln\left(\frac{1}{\xi}\right) + S_r^{*1-\alpha}\right]^{\frac{1}{1-\alpha}} \tag{45}$$

which yields

$$\xi = \exp\left[\frac{S_r^{*1-\alpha} - S_i^{1-\alpha}}{1-\alpha}\right] \tag{46}$$

It may be observed that from this expression of ξ an additional and more practical formulation can be obtained for the radial stresses, independent of S_r^*:

$$S_r = \left[S_i^{1-\alpha} + (1-\alpha)\ln\left(\frac{r}{R}\right)\right]^{\frac{1}{1-\alpha}} \tag{47}$$

3.3. Plastic zone without edge effects: solutions for strains and displacements

Strains and displacements within the plastic zone are determined using the equations of incremental plasticity described in Section 2. As presented in Ref. 7, the plastic flow rules (17) can be combined after one derivation step with Eqs. (20)–(22) to obtain the following differential equation for displacement rates:

$$\frac{\partial \dot{u}}{\partial r} - A_1\frac{\dot{u}}{r} = \frac{1}{2\Gamma}\left(A_2\dot{S}_r - A_3\dot{S}_\theta\right) \tag{48}$$

where

$$A_1 = \frac{\partial G^P/\partial S_r}{\partial G^P/\partial S_\theta}, \quad A_2 = (1-\nu) + \nu\cdot\frac{\partial G^P/\partial S_r}{\partial G^P/\partial S_\theta}, \quad A_3 = \nu + (1-\nu)\cdot\frac{\partial G^P/\partial S_r}{\partial G^P/\partial S_\theta}$$

where G^P is the normalized plastic potential.

To solve this equation, Carranza-Torres and Fairhurst[6] proposed the use of an original method adapted from the early work of Detournay[27], which establishes that the internal radial stress S_i is not the best kinematic parameter to describe the evolution of the system and can be effectively replaced by ξ, since a monotonic relationship exists between these two parameters. Consequently, for the remainder of this paper, the operator "$\dot{}$" will indicate a derivative with respect to ξ. Furthermore, the following variable change will be used to simplify the problem:

$$\rho = \frac{r}{R\xi} \tag{49}$$

Using the various equations that describe rock mass behavior, an equivalent problem depending on only one parameter (r and ξ disappear and only ρ remains) can be defined with this variable change. Moreover, the partial differential equations are transformed into total differential equations that can be solved in closed-form. More specifically, it can be shown that the displacements necessarily take the form (see Ref. 28 for details):

$$u = \xi\cdot g(\rho) \tag{50}$$

$$\text{and} \quad \dot{u} = g(\rho) - \rho\frac{dg(\rho)}{d\rho} \tag{51}$$

where g is a function of ρ only.

This expression can be used in Eq. (48) to obtain a new differential equation:

$$\frac{d^2g(\rho)}{d\rho^2} - \frac{A_1}{\rho}\frac{dg(\rho)}{d\rho} + \frac{A_1}{\rho^2}g(\rho) = \frac{R}{2\Gamma}\left(A_2\frac{dS_r}{d\rho} - A_3\frac{dS_\theta}{d\rho}\right) \tag{52}$$

Finally, since $\frac{dS_r}{d\rho} = \frac{1}{\rho}S_r^\alpha$, and $\frac{dS_\theta}{d\rho} = \frac{1}{\rho}(S_r^\alpha + \alpha S_r^{2\alpha-1})$ calculating the displacements is reduced to a matter of solving the second order differential equation below:

$$\frac{d^2g(\rho)}{d\rho^2} - \frac{A_1}{\rho}\frac{dg(\rho)}{d\rho} + \frac{A_1}{\rho^2}g(\rho) = \frac{R}{2\rho\Gamma}\left[(A_2 - A_3)S_r^\alpha - \alpha A_3 S_r^{2\alpha-1}\right] \tag{53}$$

where $S_r = [(1-\alpha)\ln(\rho) + S_r^{*1-\alpha}]^{\frac{1}{1-\alpha}}$, and the transformed boundary conditions (36) and (37) take the form $g(1) = \frac{S_0 - S_r^*}{2\Gamma}R$ and $\frac{dg}{d\rho}(1) = g'(1) = -\frac{S_0 - S_r^*}{2\Gamma}R$.

The integration of this differential equation depends on the plastic potential. Firstly, in the case of the Mohr–Coulomb plastic potential, coefficients A1, A2, and A3 are reduced to $A_1 = -K_\psi$, $A_2 = (1-\nu) - \nu\cdot K_\psi$, and $A_3 = \nu - (1-\nu)\cdot K_\psi$, and Eq. (53) can be written as

$$\frac{d^2g(\rho)}{d\rho^2} + \frac{K_\psi}{\rho}\frac{dg(\rho)}{d\rho} - \frac{K_\psi}{\rho^2}g(\rho) = \frac{R}{2\rho\Gamma}\left[(1-2\nu)\left(K_\psi + 1\right)S_r{}^\alpha - \alpha\left(\nu - (1-\nu)K_\psi\right)S_r{}^{2\alpha-1}\right] \tag{54}$$

When $\alpha=½$, a closed-form solution can be calculated

$$g(\rho)=\frac{\rho}{A_1-1}\left(A_1 g(1)-g'(1)\right)+\frac{\rho^{A_1}}{(A_1-1)}\left(g'(1)-g(1)\right)$$
$$+\frac{\rho R}{2\Gamma(A_1-1)^3}\left\{\left(1-\rho^{A_1-1}\right)\left[(1-A_1)(A_2-A_3)\sqrt{S_r^*}+\frac{1}{2}(A_1A_3-A_2)\right]\right.$$
$$+\ln(\rho)\cdot\left[(A_1-1)^2(A_3-A_2)\left(\sqrt{S_r^*}+\frac{\ln(\rho)}{4}\right)\right.$$
$$\left.\left.+\frac{1}{2}(A_1-1)(A_3A_1-A_2)\right]\right\} \tag{55}$$

which gives similar results to the expression proposed in Ref. 7 for u.

When $\alpha\neq 0.5$, there is no closed form solution and a simple one-step numerical approach, such as the 4th-order Runge Kutta method, can be used. This involves solving the problem in a spreadsheet as described later on in Section 4.1.

Secondly, in the case of a Hoek–Brown plastic potential, coefficients A_1, A_2, and A_3 are $A_1 = -1-\alpha {S_r}^{\alpha-1}$, $A_2 = 1-2\nu-\nu\alpha {S_r}^{\alpha-1}$, and $A_3 = 2\nu-1-(1-\nu)\alpha {S_r}^{\alpha-1}$, and Eq. (53) can be written as

$$\frac{d^2g(\rho)}{d\rho^2}+\frac{1+\alpha S_r^{\alpha-1}}{\rho}\frac{dg(\rho)}{d\rho}-\frac{1+\alpha S_r^{\alpha-1}}{\rho^2}g(\rho)$$
$$=\frac{R}{2\rho\Gamma}\left[2(1-2\nu)\left(S_r^{\alpha}+\alpha S_r^{2\alpha-1}\right)+(1-\nu)\alpha^2 S_r^{3\alpha-2}\right] \tag{56}$$

Contrary to what has been stated in Ref. 7, a closed-form solution can be found to this equation when $\alpha=0.5$. The integration process is described in Appendix 2. The final result is as follows:

$$g(\rho)=\left\{2\sqrt{S_r^*}\cdot e^{4\sqrt{S_r^*}}\cdot\left[\mathrm{Ei}\left(-2\ln(\rho)-4\sqrt{S_r^*}\right)-\mathrm{Ei}\left(-4\sqrt{S_r^*}\right)\right]\right.$$
$$\left[g'(1)-g(1)-\frac{R}{2\Gamma}\left((1-2\nu)\sqrt{S_r^*}+\frac{1-\nu}{8\sqrt{S_r^*}}\right)\right]+g(1)$$
$$\left.-\frac{R}{8\Gamma}(1-\nu)\ln\left(2\sqrt{S_r^*}\right)\right\}\rho$$
$$+\frac{\rho R}{2\Gamma}\left[(1-2\nu)\ln(\rho)\sqrt{S_r^*}+\frac{1}{4}(1-2\nu)\ln(\rho)^2\right.$$
$$\left.+\frac{1}{4}(1-\nu)\ln\left(\ln(\rho)+2\sqrt{S_r^*}\right)\right] \tag{57}$$

where Ei is the exponential integral function. For other α values, the problem can be solved using the Runge-Kutta method.

The equations presented in Sections 3.2 and 3.3 allow a complete resolution of the convergence problem when no edge effects appear while decreasing σ_i. In the other cases, the set of Eq. (26) must be taken into account; a detailed calculation procedure is presented below.

3.4. Plastic zone with edge effects: solutions for stresses and edge effect radius

In the cases studied here, edge effects can only appear between the tangential (θ) and longitudinal (x) stress directions. These edge effects are characterized by $S_x=S_\theta$, which can be written, using Eqs. (40) and (6), as

$$(\nu-1)S_r^{\alpha}+(2\nu-1)S_r+(1-2\nu)S_0=0 \tag{58}$$

This equation is the "edge effect criterion". Its left part has only one positive solution, written as $\hat{S}_r$. When $S_r<\hat{S}_r$, edge effects occur around the cavity. If $\hat{S}_r<S_i$, no edge effects appear.

In the general case ($\alpha\neq$½), the $\hat{S}_r$ value can be calculated with a simple Newton–Raphson method. However, in the particular case of $\alpha=$½, the edge effect criterion can be solved directly as

$$\hat{S}_r=\frac{1}{2}\left[\left(\frac{1-\nu}{1-2\nu}\right)^2+2S_0-\left(\frac{1-\nu}{1-2\nu}\right)\sqrt{\left(\frac{1-\nu}{1-2\nu}\right)^2+4S_0}\right] \tag{59}$$

Moreover, as explained in other papers such as Ref. 29, using the axisymetric hypotheses considered here, when edge effects appear at a given point around the tunnel, they are observed up to the tunnel wall. Consequently, an "edge effect radius" $R.\zeta$, with $\zeta<\xi$, can be calculated within the plastic zone. This edge effect radius may be derived from Eq. (47) $\hat{\hat{S}}_r=[{S_i}^{1-\alpha}+(1-\alpha)\ln(\zeta)]^{\frac{1}{1-\alpha}}$, which yields

$$\zeta=\exp\left(\frac{{\hat{S}_r}^{1-\alpha}-{S_i}^{1-\alpha}}{1-\alpha}\right) \tag{60}$$

Using these results, stresses in the plastic zone can be calculated as follows when edge effects appear: first, S_r is obtained from Eq. (39) for $r<R\xi$. Next, S_θ is calculated from the failure criterion $S_\theta=S_r+{S_r}^{\alpha}$ for $r<R\xi$. Finally, S_x is obtained from Eq. (40) for $R\zeta\le r\le R\xi$ and from the relationship $S_x=S_\theta$ (edge effects) for $r<R\zeta$.

3.5. Plastic zone with edge effects: solutions for strains and displacements

This solving process is based on the one presented in Section 3.2. The following notations are used: G^P is the plastic potential, either Mohr–Coulomb or Hoek–Brown; ${G_1}^P$ is the expression of this plastic potential with principal stresses (S_θ, S_r); and ${G_2}^P$ is the expression of this plastic potential with principal stresses (S_x, S_r).

By using Eqs. (21), (22), (25) and (26), the following system can be obtained:

$$\begin{cases}\dfrac{\dot{u}}{r}-\dot{\chi}_1\dfrac{\partial G_1^P}{\partial S_\theta}=\dfrac{1}{H}\left[(1-\nu)\dot{S}_\theta-\nu\dot{S}_r\right]\\ 0-\dot{\chi}_2\dfrac{\partial G_2^P}{\partial S_x}=\dfrac{1}{H}\left[(1-\nu)\dot{S}_\theta-\nu\dot{S}_r\right]\\ \dfrac{\partial\dot{u}}{\partial r}-(\dot{\chi}_1+\dot{\chi}_2)\dfrac{\partial G^P}{\partial S_r}=\dfrac{1}{H}\left[\dot{S}_r-2\nu\dot{S}_\theta\right]\end{cases} \tag{61}$$

Next, parameters $\dot{\chi}_1$ and $\dot{\chi}_2$ can be eliminated, yielding the incremental differential equation:

$$\frac{\partial\dot{u}}{\partial r}=\frac{1}{H}\cdot\left(\dot{S}_r-2\nu\dot{S}_\theta\right)$$
$$+\frac{\partial G^P}{\partial S_r}\left\{\frac{1}{\partial G_2^P/\partial S_x}\cdot\frac{1}{H}\cdot\left[\nu\dot{S}_r-(1-\nu)\dot{S}_\theta\right]+\frac{1}{\partial G_1^P/\partial S_\theta}\right.$$
$$\left.\cdot\left[\frac{\dot{u}}{r}-\frac{1}{H}\cdot\left((1-\nu)\dot{S}_\theta-\nu\dot{S}_r\right)\right]\right\} \tag{62}$$

Note that, for both the Mohr–Coulomb and Hoek–Brown plastic potentials:

$$\frac{\partial G_1^P}{\partial S_\theta}=\frac{\partial G_2^P}{\partial S_x} \tag{63}$$

which allows the use of only one plastic potential in the calculations. In the following steps, only the plastic potential with principal stresses S_θ and S_r is retained, and is simply called G^P. Consequently, expression (62) can be simplified into

$$\frac{\partial \dot{u}}{\partial r} - \hat{A}_1 \frac{\dot{u}}{r} = \frac{1}{H}\left(\hat{A}_2 \dot{S}_r - \hat{A}_3 \dot{S}_\theta\right)$$
$$\hat{A}_1 = \frac{\partial G^P/\partial S_r}{\partial G^P/\partial S_\theta}$$
$$\hat{A}_2 = 1 + 2\nu \frac{\partial G^P/\partial S_r}{\partial G^P/\partial S_\theta}$$
$$\hat{A}_3 = 2\nu + 2(1-\nu)\frac{\partial G^P/\partial S_r}{\partial G^P/\partial S_\theta} \quad (64)$$

This equation has the same form as Eq. (48), and can be solved in a similar manner. With the variable change (49) and $u=\xi g(\rho)$, calculating the displacements is reduced to solving the second order differential equation below:

$$\frac{d^2 g(\rho)}{d\rho^2} - \frac{\hat{A}_1}{\rho}\frac{dg(\rho)}{d\rho} + \frac{\hat{A}_1}{\rho^2} g(\rho) = \frac{R}{\rho H}\left[\left(\hat{A}_2 - \hat{A}_3\right) S_r^{\alpha} - \alpha \hat{A}_3 S_r^{2\alpha-1}\right] \quad (65)$$

with S_r calculated from Eq. (39).

The boundary conditions are the values of $g(\frac{\zeta}{\xi})$ and $g'(\frac{\zeta}{\xi})$, at the limit of the edge effect zone, that were calculated previously from Eq. (53).

The integration of this differential equation depends on the plastic potential. In the case of the Mohr–Coulomb plastic potential, coefficients $\hat{A}_1$ to $\hat{A}_3$ are $\hat{A}_1 = -K_\psi$, $\hat{A}_2 = 1 - 2\nu \cdot K_\psi$, $\hat{A}_3 = 2\nu - 2(1-\nu)\cdot K_\psi$, and Eq. (65) can be written as

$$\frac{d^2 g(\rho)}{d\rho^2} + \frac{K_\psi}{\rho}\frac{dg(\rho)}{d\rho} - \frac{K_\psi}{\rho^2} g(\rho) = \frac{R}{\rho H}\left[\left(1 - 2\nu + 2(1-2\nu)K_\psi\right) S_r^{\alpha} - \alpha\left(2\nu - 2(1-\nu)K_\psi\right) S_r^{2\alpha-1}\right] \quad (66)$$

In the general case ($\alpha \neq ½$), this equation has no closed-form solution and a simple 4th-order Runge-Kutta method can be used to solve the problem (see Appendix 1). However, when $\alpha = ½$, an exact solution is obtained:

$$\begin{aligned} g(\rho) = {} & \frac{\rho}{\hat{A}_1 - 1}\left(\hat{A}_1 \frac{\xi}{\zeta} g\left(\frac{\zeta}{\xi}\right) - g'\left(\frac{\zeta}{\xi}\right)\right) \\ & + \frac{\rho^{\hat{A}_1}}{\left(\hat{A}_1 - 1\right)\left(\frac{\zeta}{\xi}\right)^{\hat{A}_1 - 1}}\left(g'\left(\frac{\zeta}{\xi}\right) - \frac{\xi}{\zeta} g\left(\frac{\zeta}{\xi}\right)\right) + \frac{R\rho}{H\left(\hat{A}_1 - 1\right)} \\ & \cdot\left\{\left[\left(\hat{A}_2 - \hat{A}_3\right)\left(\sqrt{S_r^*} + \frac{1}{4}\ln\left(\frac{\zeta}{\xi}\right)\right) - \frac{\hat{A}_3}{2}\right]\ln\left(\frac{\zeta}{\xi}\right) - \right. \\ & \left[\left(\hat{A}_2 - \hat{A}_3\right)\left(\sqrt{S_r^*} + \frac{1}{4}\ln(\rho)\right) + \frac{\hat{A}_2 - \hat{A}_1\hat{A}_3}{2\left(\hat{A}_1 - 1\right)}\right]\ln(\rho) \\ & \left. - \frac{\hat{A}_2 - \hat{A}_3}{\hat{A}_1 - 1}\sqrt{S_r^*} - \frac{\hat{A}_2 - \hat{A}_1\hat{A}_3}{2\left(\hat{A}_1 - 1\right)^2}\right\} \\ & + \frac{R\rho^{\hat{A}_1}}{H\left(\hat{A}_1 - 1\right)\left(\frac{\zeta}{\xi}\right)^{\hat{A}_1 - 1}}\left[\frac{\hat{A}_2 - \hat{A}_3}{2\left(\hat{A}_1 - 1\right)}\ln\left(\frac{\zeta}{\xi}\right)\right. \\ & \left. + \frac{\hat{A}_2 - \hat{A}_3}{\hat{A}_1 - 1}\sqrt{S_r^*} + \frac{\hat{A}_2 - \hat{A}_1\hat{A}_3}{2\left(\hat{A}_1 - 1\right)^2}\right] \end{aligned} \quad (67)$$

In the case of a Hoek–Brown plastic potential, coefficients $\hat{A}_1$ to $\hat{A}_3$ are $\hat{A}_1 = -1 - \alpha S_r^{\alpha-1}$, $\hat{A}_2 = 1 - 2\nu(1 + \alpha S_r^{\alpha-1})$, and $\hat{A}_3 = 2\nu - 2(1-\nu)(1 + \alpha S_r^{\alpha-1})$, and Eq. (65) can be written as

$$\frac{d^2 g(\rho)}{d\rho^2} + \frac{1 + \alpha S_r^{\alpha-1}}{\rho}\frac{dg(\rho)}{d\rho} - \frac{1 + \alpha S_r^{\alpha-1}}{\rho^2} g(\rho) = \frac{R}{\rho H}\left[(1-2\nu)\left(3S_r^{\alpha} + 4\alpha S_r^{2\alpha-1}\right) + 2(1-\nu)\alpha^2 S_r^{3\alpha-2}\right] \quad (68)$$

This equation is similar to Eq. (56) and can be solved in the same way. Following the process described in Appendix 2, an exact solution is obtained for $\alpha = ½$:

$$\begin{aligned} g(\rho) = {} & \left\{\left[\mathrm{Ei}\left(-2\ln(\rho) - 4\sqrt{S_r^*}\right) - \mathrm{Ei}\left(-2\ln\left(\frac{\zeta}{\xi}\right) - 4\sqrt{S_r^*}\right)\right]\right. \\ & \cdot C_4 + C_5 + \frac{R}{2H}\left[\frac{3}{4}(1-2\nu)\ln\right. \\ & (\rho)^2 + (1-2\nu)\left(3\sqrt{S_r^*} + \frac{1}{2}\right)\ln(\rho) \\ & \left.\left. + \frac{3-2\nu}{4}\ln\left(\ln(\rho) + 2\sqrt{S_r^*}\right)\right]\right\}\rho \end{aligned} \quad (69)$$

where Ei is again the exponential integral function. Parameters C_4 and C_5 are calculated with the values of $g(\frac{\zeta}{\xi})$ and $g'(\frac{\zeta}{\xi})$ at the limit of the edge effect zone:

$$\begin{aligned} C_4 = {} & -\frac{e^{4\sqrt{S_r^*}}}{2H}\left(\frac{\zeta}{\xi}\right)^2\left\{2H\left(\ln\left(\frac{\zeta}{\xi}\right) + 2\sqrt{S_r^*}\right)\left(\frac{\xi}{\zeta}\cdot g\left(\frac{\zeta}{\xi}\right) - g'\left(\frac{\zeta}{\xi}\right)\right)\right. \\ & + \frac{3-2\nu}{4}R + (1-2\nu)R\left[\sqrt{S_r^*} + 6S_r^* + \frac{3}{2}\ln\left(\frac{\zeta}{\xi}\right)^2\right. \\ & \left.\left. + \frac{1 + 12\sqrt{S_r^*}}{2}\ln\left(\frac{\zeta}{\xi}\right)\right]\right\} \end{aligned}$$

$$\begin{aligned} C_5 = {} & \frac{\xi}{\zeta}\cdot g\left(\frac{\zeta}{\xi}\right) - \frac{R}{2H}\left[\frac{3}{4}(1-2\nu)\ln\left(\frac{\zeta}{\xi}\right)^2 + (1-2\nu)\left(3\sqrt{S_r^*} + \frac{1}{2}\right)\ln\left(\frac{\zeta}{\xi}\right)\right. \\ & \left. + \frac{3-2\nu}{4}\ln\left(\ln\left(\frac{\zeta}{\xi}\right) + 2\sqrt{S_r^*}\right)\right] \end{aligned}$$

For other values of α, Eq. (68) can be solved in a spreadsheet with a 4th-order Runge Kutta method.

With these last equations, the complete solution for tunnel convergence in a rock mass that satisfies the generalized Hoek–Brown criterion is now available, whether edge effects appear or not. The next section explains how these results may be used in practice. It also presents a validation by comparing them with finite element calculations.

4. Implementation and validation of the analytical solutions

4.1. Implementing the solutions

Despite their apparent complexity, the analytical solutions developed in the previous sections can be implemented very simply in a spreadsheet. This is an important step, as it provides the engineer with easy access to calculation results for the purpose of tunnel design. To do this (in the general elasto-plastic case), the authors suggest the following process, which has proven to be highly effective (see Section 4.2):

1- Calculation of the adimensional values: S_0, S_i, Γ, and H from the

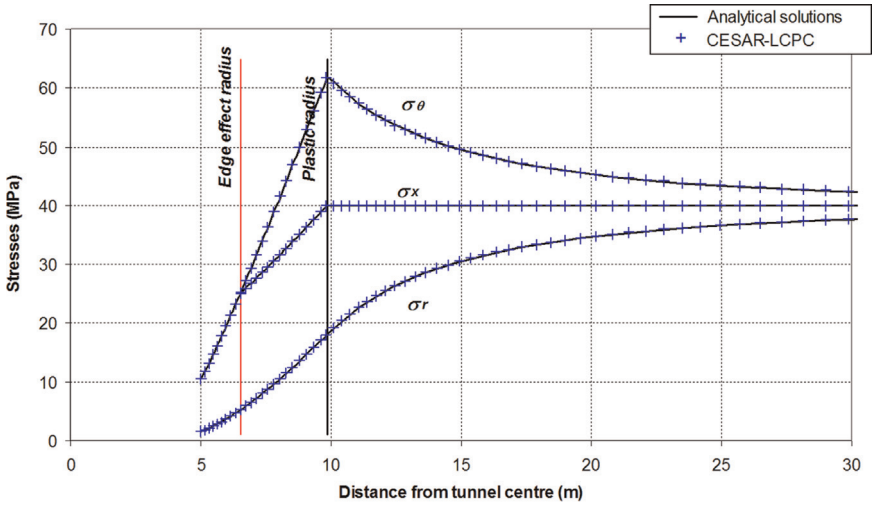

Fig. 4. Comparison of radial (σ_r), tangential (σ_θ) and longitudinal (σ_x) stress values between analytical and numerical calculations.

initial field conditions as presented in Fig. 2, and from the parameters m, s, σ_{ci}, and α of the failure criterion;

2- Calculation of the stress value S_r^* at the elastic/plastic limit, by solving Eq. (42), either in closed-form when $\alpha=½$ or using the Newton–Raphson method otherwise. Calculation of the plastic radius $R\xi$ with expression (46).

3- Verification of the occurrence of edge behaviors using the edge effect criterion (58). If necessary, calculation of the edge radius $R\zeta$ with expression (60).

4- Calculation of stresses, strains and displacements in the elastic zone using equations (29)–(34).

5- Discretization of the plastic zone using step h, and the edge effect zone using step $\hat{h}$. Calculation of $\rho=r/(R\xi)$ values at each radius step.

6- Calculation of the normalized stresses in the plastic zone ($r<R\xi$):
   - S_r from Eq. (47);
   - S_θ from the normalized failure criterion $S_\theta=S_r+S_r^{\alpha}$;
   - S_x from (40) when $R\zeta \le r \le R\xi$ and from $S_x=S_\theta$ when $r<R\zeta$.

7- Calculation of the displacements in the plastic zone without edge effects ($R\zeta \le r \le R\xi$). When $\alpha=½$, closed-form solutions (55) or (57) can be used. In the other cases, differential equation (53) can be solved using the fourth-order Runge-Kutta method in Appendix 1 with

$$t=\rho \quad t_0=1 \quad h_j=h \quad y=g \quad \dot{y}=\frac{dg}{d\rho} \quad \ddot{y}=\frac{d^2g}{d\rho^2} \quad y_0=g(1) \quad \dot{y}_0=g'(1)$$

$$f\left(\rho, g(\rho), \frac{dg(\rho)}{d\rho}\right) = \frac{A_1}{\rho}\frac{dg(\rho)}{d\rho} - \frac{A_1}{\rho^2}g(\rho) + \frac{R}{2\rho\Gamma}\left[(A_2-A_3)S_r{}^{\alpha} - \alpha A_3 S_r{}^{2\alpha-1}\right]$$

The displacement u is obtained at each radius step by $u=\xi\, g(\rho)$.

8- Calculation of the displacements in the plastic zone with edge effects ($r<R\zeta$). When $\alpha=½$ the exact solutions given by Eq. (67) or (69) can be used. In the other cases, differential equation (65) can be solved with the fourth-order Runge-Kutta method in Appendix 1 with

$$t=\rho \quad t_0=\frac{\zeta}{\xi} \quad h_j=\hat{h} \quad y=g \quad \dot{y}=\frac{dg}{d\rho} \quad \ddot{y}=\frac{d^2g}{d\rho^2} \quad y_0=g\left(\frac{\zeta}{\xi}\right) \quad \dot{y}_0=g'\left(\frac{\zeta}{\xi}\right)$$

$$f\left(\rho, g(\rho), \frac{dg(\rho)}{d\rho}\right) = \frac{\hat{A}_1}{\rho}\frac{dg(\rho)}{d\rho} - \frac{\hat{A}_1}{\rho^2}g(\rho) + \frac{R}{\rho H}\left[\left(\hat{A}_2-\hat{A}_3\right)S_r{}^{\alpha} - \alpha\hat{A}_3 S_r{}^{2\alpha-1}\right]$$

The boundary conditions y_0 and $\dot{y}_0$ at $\rho=\zeta/\xi$ are calculated from step 7-.

The displacement u is obtained at each radius step by $u=\xi.g(\rho)$.

9- Calculation of strains in the plastic zone (with and without edge effects) for each radius step: tangential strains can be obtained using relation (22) and radial strains using:

$$\varepsilon_r = \frac{\partial u(r,\xi)}{\partial r} = \frac{1}{R\xi}\frac{d(\xi\cdot g(\rho))}{d\rho} = \frac{1}{R}\frac{dg(\rho)}{d\rho} \tag{70}$$

A spreadsheet of this type has been programmed by the authors of this paper to execute the calculations presented in the next section (and others); it can be obtained at no cost by contacting the authors.

4.2. Validation

The closed-form solutions described in the previous sections can be validated in several ways. One method consists of comparing them with existing solutions in the literature (when possible). In particular, the results of 7 can be used in some calculation cases that include no edge effects. In other cases, comparison with finite element calculations can be used.

The finite element calculations were performed with CESAR-LCPC software using a 1D-axisymmetric model. The excavation was simulated by applying deconfinement stresses on one side of the model, while infinite elements were positioned on the other side. The model was composed of quadrangular elements with a quadratic interpolation between Gauss points. The thinner elements near the tunnel wall had a thickness of 10 cm.

Below, some comparison results are shown for the following configuration: a tunnel radius $R=5$ m, an initial isotropic far-field stress value $\sigma_0=40$ MPa and a final confining stress at the tunnel wall $\sigma_i=1.5$ MPa. The chosen parameters for the Hoek–Brown failure criterion refer to a highly tectonized quartzitic sandstone as described in 30: $m=2.48$, $s=0.00024$, $\sigma_{ci}=42$ MPa, $\alpha=0.64$. The elastic parameters are set at $E=3$ GPa (Young's modulus) and $\nu=0.3$ (Poisson ratio). The plastic flow rule is characterized by a dilatancy angle of $\psi=10°$.

The plastic radius, as well as the radial and tangential stresses when no edge effects appear, can be validated directly, since in this case the expressions presented in this paper are similar to those of 7 (with a difference in stress normalization alone; see relation (3)).

With regard to the intermediate stress σ_x and the edge effect radius $R\zeta$, some comparisons were made using CESAR-LCPC calculations. Fig. 4 shows the excellent correspondence between

Table 1
Values of displacements, plastic radius and edge effect radius calculated using various methods (values in italics were obtained via linear interpolation between two integration points).

Values in m	Mohr–Coulomb plastic potential ($\psi=10°$)						Associated Hoek–Brown plastic potential				
	$\alpha=0.5$			$\alpha=0.64$			$\alpha=0.5$			$\alpha=0.64$	
	FR-E	FR-RK	CESAR	FR-RK	CCT	CESAR	FR-E	FR-RK	CESAR	FR-RK	CESAR
$R.\xi$	9.076	9.076	*9.068*	9.856	9.856	*9.838*	9.076	9.076	*9.068*	9.856	*9.839*
$R.\zeta$	5.833	5.833	*5.845*	6.527	–	*6.496*	5.833	5.833	*5.787*	6.527	*6.496*
u(15 m)	0.052	0.052	*0.052*	0.062	0.062	*0.062*	0.052	0.052	*0.052*	0.062	*0.062*
$u(R.\xi)$	0.086	0.086	*0.086*	0.094	0.094	*0.094*	0.086	0.086	*0.086*	0.094	*0.094*
$u(R.\zeta)$	0.168	0.168	*0.168*	0.176	*0.176*	*0.178*	0.229	0.229	*0.233*	0.254	*0.257*
$u(R)$	0.220	0.220	0.220	0.280	–	0.280	0.391	0.391	0.378	0.668	0.648

analytical and numerical results.

With regard to displacements, Table 1 shows some displacement values obtained with the calculation parameters presented previously, with two possible values for α (either 0.5 or 0.64). The dilatancy ψ is used only in the non-associated case. Some edge effects appear in these cases, as shown in Fig. 4.

The following abbreviations are used in Table 1. Results 'FR-RK' are from the analytical methods presented in this paper, with a final integration using the Runge-Kutta process. Results 'FR-E' are also from the analytical methods presented in this paper but with exact solutions (only for $\alpha=0.5$). Results 'CCT' are from calculations with the spreadsheet from Ref. 7. Results 'CESAR' are from finite element calculations with the CESAR-LCPC software.

This table shows a high degree of agreement among the various calculation methods. In the case of $\alpha=0.5$, though only 3 significant digits are displayed in Table 1, in reality differences between the exact solutions and the Runge-Kutta integration appear only after 7 digits. The numerical values from CESAR-LCPC are also very similar to the theoretical ones, especially in the case of a Mohr–Coulomb plastic potential. In the case of an associated flow rule, the values are very good even if they differ from analytical solutions by 2–3 percent. This difference in precision can be explained by the calculation of the plastic potential derivative, which is performed at the elastic estimator in CESAR-LCPC and not at the exact contact point with the failure criterion. This introduces a slight bias for an associated flow rule, which does not exist in the case of a linear Mohr–Coulomb potential.

It is also interesting to note in Table 1 that significant differences may appear for convergence at the tunnel wall between an associated and a non-associated flow rule. These results clearly highlight the importance of an appropriate plastic potential choice for design-oriented calculations.

5. Conclusions

The calculations presented in this paper constitute a comprehensive method for the calculation of stresses and displacement around tunnels in rock masses obeying the generalized Hoek–Brown criterion. The calculations are based notably on previous work by Carranza-Torres et al. and take rigorously into account the various mechanical equations.

Several innovations have been made compared to existing solutions in the literature. Firstly, a new dimensionless form of the generalized Hoek–Brown failure criterion based on a new stress normalization, Eq. (3), has been established, which simplified previously existing solutions for tunnel convergence. In addition, the convergence calculations have been completed by taking into account the problem of edge effects, which were not previously addressed in the literature. Furthermore, in the case of an associated Hoek–Brown plastic potential, new exact formulations have been obtained for the case of α =½, which was considered unsolvable until now.

All the developments made in this paper have been validated by comparisons with existing solutions in the literature (when possible) or with finite element CESAR-LCPC calculations. Finally, the formulations presented here yield excellent results. They can be easily implanted into spreadsheets, allowing direct use in an engineering study, for example.

This paper is a first step for a complete resolution of stresses and displacements around a tunnel, in the axisymmetric case, within a generalized Hoek–Brown rock mass. The authors have used the same methodology to develop additional exact solutions when the effects of water must be taken into account, in drained and undrained situations. These types of developments are particularly useful in the case of intermediate materials such as hard soils or soft rocks and shall be presented in a subsequent article.

Acknowledgments

The authors wish to thank the French Ministry for Ecology and Sustainable Development and the Regional Laboratory of Toulouse for their support of this project; the Centre for Tunnel Studies for its review; and Dr E. Bourgeois (French institute of science and technology for transport, development and networks) for his assistance in the use of CESAR-LCPC software.

Appendix 1. : 4th order Runge Kutta method used in this paper

The Runge-Kutta method used in this paper is an adaptation of the classical method for first-order differential equations to second-order ones. It can be found for instance in Ref. 27.

The solving process applies to Cauchy problems of the form

$$t\begin{cases}\ddot{y}=f\left(t,y(t),\dot{y}(t)\right)\\ y\left(t_0\right)=y_0\\ \dot{y}\left(t_0\right)=\dot{y}_0\end{cases} \tag{71}$$

where t is the derivation variable defined on an interval $I\in\mathbb{R}$, y yields values in $\mathbb{R}^p$ ($p=1$ in the cases studied here), $\dot{y}$ is the first derivative of y with respect to t, $\ddot{y}$ the second derivative of y with respect to t, and f is a continuous function on $I\times\mathbb{R}^p$.

The interval $I=[t_0;\ t_0+T]$ is subdivided into n points $t_0<t_1<\ldots<t_n=t_0+T$, which define steps $h_j=t_{j+1}-t_j$. At each point t_j, the function y can be approximated by a value $y_j\approx y(t_j)$.

For the Cauchy problem presented previously, the following relationships can be written to integrate the differential equation:

$$\begin{cases} y_{j+1} = y_j + h_j\,\Phi_1\left(t_j \dot{y}_j, y_j, h_j\right) \\ \dot{y}_{j+1} = \dot{y}_j + h_j\,\Phi_2\left(t_j \dot{y}_j, h_j\right) \\ y_0 \text{ and } \dot{y}_0 = \text{approximation of initial conditions} \end{cases} \tag{72}$$

with

$$\begin{cases} \Phi_1(t, \dot{y}, y, h) = \dot{y} + \dfrac{h}{6}(k_1 + k_2 + k_3) \\ \Phi_2(t, \dot{y}, h) = \dfrac{1}{6}(k_1 + 2k_2 + 2k_3 + k_4) \end{cases} \tag{73}$$

$$k_1 = f(t, y, \dot{y})$$

$$k_2 = f\left(t + \frac{h}{2}, y + \frac{h}{2}\dot{y} + \frac{h^2}{8}k_1, \dot{y} + \frac{h}{2}k_1\right)$$

$$k_3 = f\left(t + \frac{h}{2}, y + \frac{h}{2}\dot{y} + \frac{h^2}{8}k_1, \dot{y} + \frac{h}{2}k_2\right)$$

$$k_4 = f\left(t + h, y + h\dot{y} + \frac{h^2}{2}k_3, \dot{y} + hk_3\right)$$

Appendix 2. : Integration steps for the case of an associated flow rule with $\alpha = 0.5$

This appendix explains the exact integration of Eq. (56) (conventional Hoek–Brown failure criterion and associated flow rule), for which no solution previously existed in the literature. When $\alpha = ½$, Eq. (56) becomes

$$\frac{d^2g(\rho)}{d\rho^2} + \left(1 + \frac{1}{\ln(\rho) + 2\sqrt{S_r^*}}\right)\frac{1}{\rho}\frac{dg(\rho)}{d\rho} - \left(1 + \frac{1}{\ln(\rho) + 2\sqrt{S_r^*}}\right)\frac{1}{\rho^2}g(\rho)$$

$$= \frac{R}{2\rho\Gamma}\left[(1 - 2\nu)\left(\ln(\rho) + 2\sqrt{S_r^*} + 1\right) + \frac{1}{2}\frac{1 - \nu}{\ln(\rho) + 2\sqrt{S_r^*}}\right] \tag{74}$$

A2.1 Solution of the equation with no second member ("ENSM")

To solve the ENSM, two linearly independent solutions have to be identified. First, $g_1(\rho) = \rho$ is an obvious solution of the ENSM. A second solution can be sought in form $g_2(\rho) = \rho \cdot f_1(\rho)$. The following result is obtained:

$$f_1(\rho) = \tilde{C}_1 \cdot e^{4\sqrt{S_r^*}} \cdot \mathrm{Ei}\left(-2\ln(\rho) - 4\sqrt{S_r^*}\right) + \tilde{C}_2 \tag{75}$$

where $\tilde{C}_1$ and $\tilde{C}_2$ are integration constants, and Ei is the Exponential Integral function, defined by the following integral:

$$\mathrm{Ei}(x) = -\int_{-x}^{\infty} \frac{e^{-t}}{t}\,dt \tag{76}$$

which must be understood as a principal Cauchy value, as $1/t$ has a singularity at $t = 0$. The values of this function can be estimated by

$$\mathrm{Ei}(x) = \gamma_{EM} + \ln(x) - \sum_{k=1}^{\infty} \frac{(-1)^{k+1}(-x)^k}{k \cdot k!} \tag{77}$$

where γ_{EM} is the Euler–Mascheroni constant:

$$\gamma_{EM} = \lim_{n\to\infty}\left(\sum_{k=1}^{n}\frac{1}{k} - \ln(n)\right) \approx 0.57721566490153286...$$

The second solution for the ENSM is obtained by choosing the constant values $\tilde{C}_1$ and $\tilde{C}_2$ so that $g_2(1) = 0$:

$$g_2(\rho) = \left[\mathrm{Ei}\left(-2\ln(\rho) - 4\sqrt{S_r^*}\right) - \mathrm{Ei}\left(-4\sqrt{S_r^*}\right)\right]\cdot\rho \tag{78}$$

Since solutions g_1 and g_2 are linearly independent, the general solution of the ENSM can be written as a linear combination of these two particular solutions:

$$g_0(\rho) = \left(\left[\mathrm{Ei}\left(-2\ln(\rho) - 4\sqrt{S_r^*}\right) - \mathrm{Ei}\left(-4\sqrt{S_r^*}\right)\right]\cdot\tilde{C}_3 + \tilde{C}_4\right)\rho \tag{79}$$

where $\tilde{C}_3$ and $\tilde{C}_4$ are integration constants to be determined from the initial conditions.

A2.2 Specific solution for equation with second member ("EWSM")

A specific solution for the EWSM can be sought in the form of $g_p(\rho) = \rho \cdot f_3(\rho)$. In this case, with $f_4(\rho) = \frac{df_3(\rho)}{d\rho}$, the initial differential Eq. (74) yields

$$\rho\frac{df_4(\rho)}{d\rho} + \left(3 + \frac{1}{\ln(\rho) + 2\sqrt{S_r^*}}\right)f_4(\rho) = \frac{R}{2\rho\Gamma}\left[(1 - 2\nu)\left(\ln(\rho) + 2\sqrt{S_r^*} + 1\right) + \frac{1}{2}\frac{1 - \nu}{\ln(\rho) + 2\sqrt{S_r^*}}\right] \tag{80}$$

This equation can be solved as follows. First, the general solution for equation with no second member (with $\tilde{C}_5$ an integration constant) is

$$f_{4,0}(\rho) = \frac{\tilde{C}_5}{\rho^3\left(\ln(\rho) + 2\sqrt{S_r^*}\right)} \tag{81}$$

A particular solution for the equation is sought in the form of

$$f_{4,p}(\rho) = \frac{f_5(\rho)}{\rho^3\left(\ln(\rho) + 2\sqrt{S_r^*}\right)} \tag{82}$$

Inserting $f_{4,p}(\rho)$ in Eq. (80) gives

$$\frac{df_5(\rho)}{d\rho} = \frac{\rho R}{2\Gamma}\left[(1 - 2\nu)\left(\ln(\rho) + 2\sqrt{S_r^*} + 1\right)\left(\ln(\rho) + 2\sqrt{S_r^*}\right) + \frac{1}{2}(1 - \nu)\right] \tag{83}$$

which can be easily integrated into (with $\tilde{C}_6$ an integration constant):

$$f_5(\rho) = \frac{R\rho^2}{\Gamma}\left[(1 - 2\nu)\left(\frac{\ln(\rho)^2}{4} + \sqrt{S_r^*}\ln(\rho) + S_r^*\right) + \frac{1 - \nu}{8}\right] + \tilde{C}_6 \tag{84}$$

Consequently, a particular solution of Eq. (80) is

$$f_{4,p}(\rho) = \frac{R}{\Gamma\rho\left(\ln(\rho) + 2\sqrt{S_r^*}\right)}\left[(1 - 2\nu)\left(\frac{\ln(\rho)^2}{4} + \sqrt{S_r^*}\ln(\rho) + S_r^*\right) + \frac{1 - \nu}{8}\right] \tag{85}$$

And by choosing $\tilde{C}_5 = 0$, a particular solution of (74) is obtained ($g_p(\rho) = \rho \cdot \iint f_{4,p}(\rho)d\rho$):

$$g_p(\rho) = \frac{\rho R}{2\Gamma}\Big[(1-2\nu)\ln(\rho)\sqrt{S_r^*} + \frac{1}{4}(1-2\nu) \ln(\rho)^2 + \frac{1}{4}(1-\nu)\ln\Big(\ln(\rho) + 2\sqrt{S_r^*}\Big)\Big] \quad (86)$$

Finally, the general solution of Eq. (74) is

$$g(\rho) = \Big(\Big[\mathrm{Ei}\Big(-2\ln(\rho) - 4\sqrt{S_r^*}\Big) - \mathrm{Ei}\Big(-4\sqrt{S_r^*}\Big)\Big]\cdot\tilde{C}_3 + \tilde{C}_4\Big)\rho + \frac{\rho R}{2\Gamma}\Big[(1-2\nu)\ln(\rho)\sqrt{S_r^*} + \frac{1}{4}(1-2\nu)\ln(\rho)^2 + \frac{1}{4}(1-\nu)\ln\Big(\ln(\rho) + 2\sqrt{S_r^*}\Big)\Big] \quad (87)$$

A2.3 Exact solution that fits the initial conditions

The exact solution must also obey the initial conditions for $\rho=1$, defined by the values of $g(1)$ and $g'(1) = \frac{dg}{d\rho}(1)$. Deriving expression (87) yields

$$\begin{cases} g(1) = \tilde{C}_4 + \dfrac{R}{8\Gamma}(1-\nu)\ln\Big(2\sqrt{S_r^*}\Big) \\ g'(1) = \tilde{C}_4 + \dfrac{R}{8\Gamma}(1-\nu)\ln\Big(2\sqrt{S_r^*}\Big) + \dfrac{R}{2\Gamma}\Big((1-2\nu)\sqrt{S_r^*} + \dfrac{1-\nu}{8\sqrt{S_r^*}}\Big) + \dfrac{e^{-4\sqrt{S_r^*}}}{2\sqrt{S_r^*}}\tilde{C}_3 \end{cases} \quad (88)$$

and then

$$\begin{cases} \tilde{C}_4 = g(1) - \dfrac{R}{8\Gamma}(1-\nu)\ln\Big(2\sqrt{S_r^*}\Big) \\ \tilde{C}_3 = 2\sqrt{S_r^*}\cdot e^{4\sqrt{S_r^*}}\cdot\Big[g'(1) - g(1) - \dfrac{R}{2\Gamma}\Big((1-2\nu)\sqrt{S_r^*} + \dfrac{1-\nu}{8\sqrt{S_r^*}}\Big)\Big] \end{cases} \quad (89)$$

References

1 Magnan J-P. Le rôle de l'expérience dans la pratique de la géotechnique. *Rev Fr Géotech.* 2005:59–66.
2 Brown ET, Bray JW, Ladanyi B, Hoek E. Ground response curves for rock tunnels. *ASCE J Geotech Eng.* 1983;109:15–39.
3 Fenner R. Undersuchungen zur Erkenntnis des Gebirgsdruckes. *Gluckhauf.* 1938;74(681–695)705–715.
4 Marinos P, Hoek E. Estimating the geotechnical properties of heterogeneous rock masses such as Flysch. *Bull Eng Geol Environ.* 2001;60:85–92.
5 Habimana J, Labiouse V, Descoeudres F. Geomechanical characterisation of cataclastic rocks: experience from the Cleuson–Dixence project. *Int J Rock Mech Min Sci.* 2002;39:677–693.
6 Carranza-Torres C, Fairhust C. The elasto-plastic response of underground excavations in rock masses that satisfy the Hoek–Brown failure criterion. *Int J Rock Mech Min Sci.* 1999;36:777–809.
7 Carranza-Torres C. Elastoplastic solution of tunnel problems using the generalized form of the Hoek–Brown failure criterion. *Int J Rock Mech Min Sci.* 2004;41:480–481.
8 Sharan SK. Elastic–brittle–plastic analysis of circular openings in Hoek–Brown media. *Int J Rock Mech Min Sci.* 2003;40:817–824.
9 Sharan SK. Exact and approximate solutions for displacements around circular openings in elastic–brittle–plastic Hoek–Brown rock. *Int J Rock Mech Min Sci.* 2005;42:542–549.
10 Sharan SK. Analytical solutions for stresses and displacemnts around a circular opening in a generalized Hoek–Brown rock. *Int J Rock Mech Min Sci.* 2008;45:78–85.
11 Serrano A, Olalla C, Reig I. Convergence of circular tunnels in elastoplastic rock masses with non-linear failure criteria and non-associated flow laws. *Int J Rock Mech Min Sci.* 2011;48:878–887.
12 Gärber R. *Design of Deep Galleries in Low Permeable Saturated Porous Media.* Lausanne: EPFL; 2003.
13 Panet M. *Le Calcul des Tunnels par la Méthode Convergence-Confinement.* Paris: Presses de l'Ecole Nationale des Ponts et Chaussées; 1995.
14 Chern JC, Shiao FY, Yu CW. An empirical safety criterion for tunnel construction. In: *Proceedings Regional Symposium on Sedimentary Rock Engineering.* Taipei, Taiwan; 1998:222–227.
15 AFTES. La méthode convergence-confinement. *Tunnels et Ouvrages Souterrains*; 2002:79–89.
16 Hoek E. *Practical Rock Engineering*. 2007 ed.: Rocscience ⟨http://www.rocscience.com/hoek/PracticalRockEngineering.asp⟩; 2007.
17 Carranza-Torres C, Fairhust C. Application of the convergence-confinement method of tunnel design to rock masses that satisfy the Hoek–Brown failure criterion. *Tunn Undergr Space Technol.* 2000;15:187–213.
18 Vlachopoulos N, Diederichs MS. Improved longitudinal displacement profiles for convergence confinement analysis of deep tunnels. *Rock Mech Rock Eng.* 2009;42:131–146.
19 Corbetta F, Bernaud D, Nguyen Minh D. Contribution à la méthode convergence-confinement par le principe de similitude. *Rev Fr Géotech.* 1991:5–11.
20 Bernaud D., Benamar I., Rousset G. La "nouvelle méthode implicite" pour le calcul des tunnels dans les milieux élastoplastiques et viscoplastiques. Rev Fr Géotech; 1994.
21 Nguyen Minh D, Guo C. A ground-support interaction principle for constant rate advancing tunnels. In: Riberiro, Sousa, Grossmann, eds. *Eurock'93, 2nd Eurock Conference*. Lisboa, Portugal; 1993.
22 Londe P. Discussion on The determination of the shear stress failure in rock masses. *ASCE J Geotech Eng Div.* 1988;114:374–376.
23 Pan XD, Hudson JA. A simplified three-dimensional Hoek–Brown yield criterion. In: Romana M, editor. Rotterdam, Netherlands: Balkema; 1988. p. 95–103.
24 Descoeudres F. *Géomécanique-Notes de cours-Chap. 4.* Lausanne: EPFL; 2001.
25 Lamé MG. *Leçons sur la théorie mathématique de l'élasticité des corps solides.* 2 ed.,Paris: Gauthier-Villars; 1866.
26 Sofianos AI, Nomikos PP. Equivalent Mohr–Coulomb and generalized Hoek–Brown strength parameters for supported axisymmetric tunnels in plastic or brittle rock. *Int J Rock Mech Min Sci.* 2006;43:683–704.
27 Detournay E. Elastoplastic model of a deep tunnel for a rock with variable dilatancy. *Rock Mech Rock Eng.* 1986;19:99–108.
28 Rojat F. *Comportement des Tunnels dans les Milieux Rocheux de Faibles Caractéristiques Mécaniques.* Marne-la-Vallée: Ecole Nationale des Ponts et Chaussées; 2010.
29 Corbetta F. *Nouvelles Méthodes d'étude des Tunnels Profonds.* Ecole Nationale Supérieure des Mines de Paris; 1990.
30 Habimana J. *Caractérisation Géomécanique de Roches Cataclastiques Rencontrées dans des Ouvrages Souterrains Alpins.* Lausanne: EPFL; 1999.